Solar Energy Materials & Solar Cells 119 (2013) 26–35

Contents lists available at ScienceDirect

Solar Energy Materials & Solar Cells

journal homepage: www.elsevier.com/locate/solmat

Remarkable progress in thin-film silicon solar cells using high-efficiency triple-junction technology

Soohyun Kim, Jin-Won Chung, Hyun Lee, Jinhee Park, Younho Heo, Heon-Min Lee *

Materials & Components R&D Laboratory, LG Electronics Advanced Research Institute, Seoul 137-724 Republic of Korea

ARTICLE INFO

Available online 15 May 2013

Keywords:
Thin-film silicon solar cell
Amorphous silicon
Microcrystalline silicon
Triple junction
Microcrystalline silicon oxide
Stabilized efficiency

ABSTRACT

Despite the many advantages of thin-film silicon (Si) solar cells, their low efficiencies remain a challenge that must be overcome. Efficient light utilization across the solar spectrum is required to achieve efficiencies over 15%, allowing them to be competitive with other solar cell technologies. To produce high-efficiency thin-film Si solar cells, we have developed triple-junction solar cell structures to enhance solar spectrum utilization. To maximize the light management, in-house ZnO:Al layers with high haze ratios and high transmittances were developed. In addition, novel doping layers, such as n-type microcrystalline silicon oxide (μc-SiO_x:H), which has a very low refractive index, and p-type microcrystalline silicon oxide (μc-SiO_x:H), which has a wide bandgap, were successfully applied to the optical reflector and the window layer, respectively. Thin-film quality control techniques for the deposition of hydrogenated amorphous silicon (a-Si:H) in the top cell, hydrogenated amorphous silicon-germanium (a-SiGe:H) or hydrogenated microcrystalline silicon (μc-Si:H) in the middle cell, and hydrogenated microcrystalline silicon (μc-Si:H) in the bottom cell were also important factors leading to the production of high-efficiency triple-junction solar cells. As a result of this work, an initial efficiency of 16.1% (in-house measurement) in the a-Si:H/a-SiGe:H/μc-Si:H stack and a stabilized efficiency of 13.4% (confirmed by NREL) in the a-Si:H/μc-Si:H/μc-Si:H stack were successfully achieved in a small-area triple-junction solar cell with dimensions of 1 cm × 1 cm.

1. Introduction

The electricity cost for solar power generation continues to decrease as a result of increasing installation of photovoltaic systems and progress in solar cell technology, which affects the manufacturing cost and conversion efficiency for solar cells, respectively. It appears that the recent plunge in the price of solar cells due to an oversupply of photovoltaic modules will make economic parity with the grid possible within 2–3 years, particularly in high-insolation areas. Meanwhile, producers of solar cells must improve solar cell efficiency and reduce manufacturing costs significantly to survive in the challenging current market environment.

Thin-film Si solar cells have received attention due to their potential for large areas and low-cost manufacturing. The abundance of raw materials makes these solar cells more attractive as a renewable energy source compared to other compound semiconductor thin-film solar cells. In addition, these solar cells exhibit a low temperature coefficient, which is especially beneficial in high-insolation areas, including the Sun Belt region. Despite the many advantages of thin-film Si solar cells, their low efficiencies still present a challenge that must be overcome. The efficiency of a single-junction amorphous Si solar panel is only 6–7%. Oerlikon Solar has demonstrated the possibility of increasing the module efficiency up to 11% by using double-junction technology, including amorphous Si (a-Si:H)/microcrystalline Si (μc-Si:H) junctions [1]. However, in our opinion, a module efficiency of 12% is necessary to be competitive with other solar cell technologies. We now believe that conventional a-Si:H/μc-Si:H double-junction solar cells will eventually be replaced by triple-junction solar cells. Triple-junction solar cells offer an even more efficient utilization of the solar spectrum by incorporating thin component cells in which the intrinsic layer materials have appropriate bandgaps for the successful absorption and collection of blue light in the top cell, green light in the middle cell, and red light in the bottom cell [2].

A conversion efficiency of 16.3% (*init.*) in a thin-film Si solar cell with an n–i–p stacked triple-junction structure (a-Si:H/a-SiGe:H/μc-Si:H) was recently reported by United Solar [3], suggesting a possible approach for exceeding the current, inadequate efficiency limit for thin-film Si solar cells. In this article, we are hoping to offer another possibility for achieving such a high efficiency by creating a p–i–n stacked triple-junction thin-film Si solar cell. Our recent progress into developing element technologies for this triple-junction solar cell and the integration technologies for the triple-junction stack will be described in detail in the sections that follow.

* Corresponding author. Tel.: +82 108 495 0815.
E-mail address: ain.lee@lge.com (H.-M. Lee).

0927-0248/$ - see front matter © 2013 Elsevier B.V. All rights reserved.
http://dx.doi.org/10.1016/j.solmat.2013.04.016

2. Element technologies for a high efficiency triple-junction solar cell

2.1. Transparent conductive oxide (TCO) as a front contact layer

The efficiency of a superstrate-type thin-film Si solar cell strongly depends on the quality of the textured TCO layer used for the front electrode material. To improve cell efficiency, it is necessary to prepare a TCO layer with a high transparency in the solar spectrum and to optimize the surface morphology for light scattering by controlling the deposition and texturing conditions. In our work, we have developed a textured ZnO:Al layer with the following characteristics: a high transparency; a high haze ratio, particularly at long wavelengths (700 nm or greater); and a U-shape surface morphology with smooth crater, which prevents the formation of cracks in the silicon layers after stacking.

The ZnO:Al layers were sputtered from an Al_2O_3 (0.5 wt %)-doped ZnO ceramic target and then chemically wet-etched with an HCl-based acid for surface texture formation. It is well-known that the sputtering pressure has a major influence on the structures of sputtered ZnO:Al layers [4] and that the subsequent texturing behavior of a ZnO:Al layer exhibits various features depending on the sputtering pressure [5]. It has been reported that low pressure sputtering conditions, below 1 mTorr, result in a significant increase in carrier mobility and a decrease in etching rate due to the formation of a dense ZnO:Al film.

To fabricate optimal ZnO:Al substrates, we varied the sputtering pressure in the range of 0.5–1.5 mTorr. Unfortunately, deposition under very low pressure often caused micro-arcing in our RF sputtering system, leading to a deterioration in the transparency of the ZnO:Al films. To produce a high-performance TCO with both high transparency and a dense structure, the sputtering pressure and time were both optimized, and, consequently, a two-step deposition process was developed successfully. For the first step, a ZnO:Al layer of 800 nm thickness was prepared at a sputtering pressure of 1 mTorr to achieve a high transparency; then, for the second step, a 0.5 mTorr sputtering pressure was applied to prepare a dense ZnO:Al film on top of this deposited film. The ZnO:Al layer prepared in the second deposition step was approximately 500 nm in thickness.

The ZnO:Al films deposited by this two-step process exhibited a smooth surface (RMS roughness 2–3 nm, determined by AFM measurement) and excellent electrical properties (carrier density $(N)=2.51\times10^{20}$ cm^{-3} and carrier mobility $(\mu)=53$ cm^2 V^{-1} s^{-1}). Each deposited ZnO:Al layer was then chemically etched in a mixture of diluted HCl and oxalic acid ($C_2H_2O_4$) to produce a textured surface morphology. As only the second ZnO:Al layer deposited was etched during this process, the thickness of the resulting textured ZnO:Al layer was approximately 800–900 nm.

Two factors that can increase the current density of a thin-film Si solar cell are high transparency and formation of an optimal light-diffusing structure in the front TCO layer. Fig. 1 compares the optical properties of commercial SnO_2:F substrates (Asahi VU) and the fabricated ZnO:Al substrates. An index-matching liquid, CH_2I_2, and a cover glass were both used to ensure that the diffuse transmittance induced by the textured TCO during the transmittance measurements could be neglected. It is clear that the transmittance of the fabricated ZnO:Al substrate is higher than that of the commercial SnO_2:F substrate at wavelengths above 700 nm. Additionally, while the haze ratio of SnO_2:F is only 2% at a wavelength of 850 nm, the fabricated ZnO:Al exhibits a significantly higher haze ratio of 48%. These enhanced optical properties for the fabricated ZnO:Al layer show potential for improving the short-circuit current of the triple-junction thin-film solar cells produced in this work, especially in the case of bottom cells that include μc-Si:H, which exhibits a very low absorption coefficient.

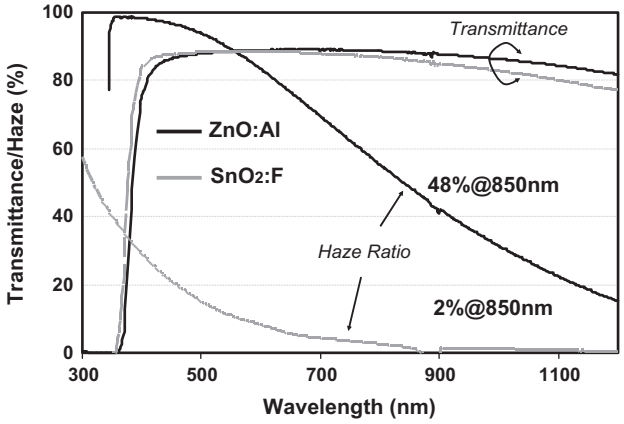

Fig. 1. Optical transmittance spectra and haze ratios of commercial SnO_2:F and fabricated ZnO:Al substrates.

It has been reported that the crystal growth of μc-Si:H on steep textures gives rise to crack formation due to collisions in columnar growth, resulting in a reduction of the open-circuit voltage (V_{oc}) and the fill factor (F.F.) [6]. The crack density can be reduced by transforming the V-shape valleys located between pyramids on the TCO surface into U-shaped valleys [7]. Therefore, the surface characteristics of TCO substrates, in addition to their optical properties, should be considered carefully. AFM topographies of the SnO_2:F and ZnO:Al substrates are shown in Fig. 2. Because the surface of the etched ZnO:Al layers exhibited U-shaped valleys with smooth craters, as shown in Fig. 2(b), the crack density in the thin-film solar cells using the ZnO:Al substrate was reduced compared to those using the SnO_2:F substrate. The TEM images for extinct cracks by U-shape valleys are not shown here, but it had similar tendency with previous other report [7]. Hereafter, all single and triple-junction solar cells in this study were prepared on the two-step deposited ZnO:Al substrates.

2.2. A high-performance a-Si:H top cell with a wide bandgap intrinsic layer

Recently, Prof. Konagai's group [2] has calculated the theoretical conversion efficiencies for triple-junction thin-film Si solar cells. These theoretical efficiencies were obtained by varying the bandgaps of the top and middle cells while fixing that of the bottom cell at 1.1 eV, corresponding to the bandgap of the bottom cell in a μc-Si:H system. According to the results of this group, the highest conversion efficiency of 21.4% was obtained when the bandgaps of the top and middle cells were 2 and 1.45 eV, respectively. Therefore, for high-efficiency triple-junction solar cells, it is very important to develop high bandgaps and high quality materials for use in the intrinsic layer of the top cell. In our work, the top cell in the triple-junction structure, the purpose of which is to absorb blue light, utilizes an a-Si:H layer with an optical bandgap of approximately 1.7 eV for its intrinsic layer.

The a-Si:H films were deposited on glass substrate via a plasma-enhanced chemical vapor deposition (PECVD) method with a radio frequency (RF) of 13.56 MHz at a substrate temperature of 180 °C. The optical parameters, such as the optical bandgap and film thickness, were determined from ellipsometry measurements by fitting the data to a Tauc–Lorentz dispersion model. Fig. 3 (a) shows the variation in the optical bandgaps of several a-Si:H layers as a function of the H_2/SiH_4 gas flow ratio and the RF power during the PECVD process. The data show that using a higher RF power slightly increases the bandgap of the a-Si:H layer, but it is clear that the H_2/SiH_4 ratio determines the bandgap level more strongly. The bandgap of a-Si:H increased with an increasing H_2

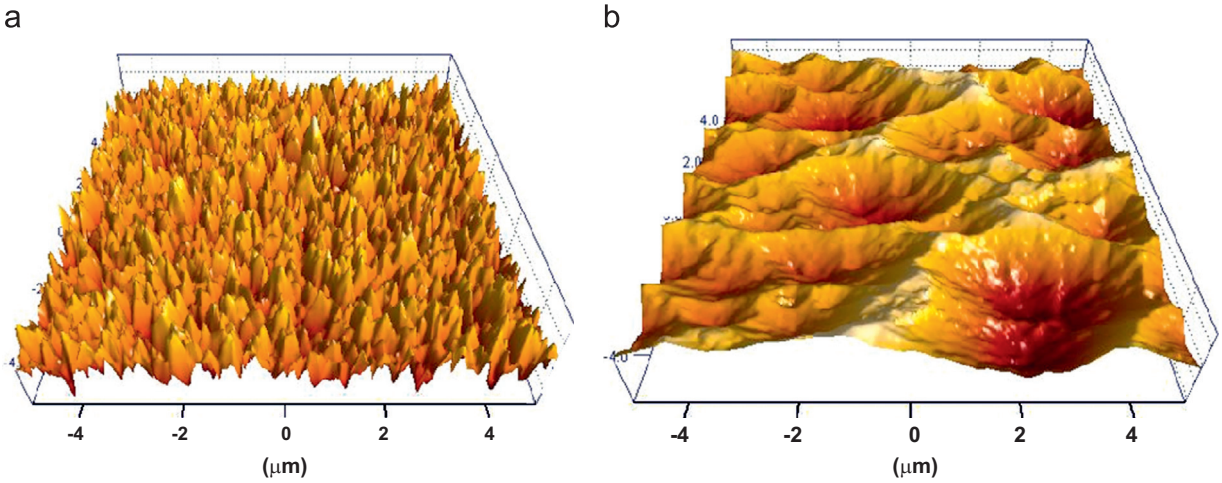

Fig. 2. AFM topographies of TCO substrates having different surface morphologies: (a) commercial SnO_2:F and (b) fabricated ZnO:Al substrate.

dilution ratio, and abruptly dropped below 1.70 eV when the H_2 dilution ratio was increased beyond 80. In this regime, the dark conductivity of the a-Si:H layer was observed to increase abruptly by over 1 order of magnitude due to a significant phase transition. This phase transition represents μc-Si:H formation within the a-Si:H matrix, as has been observed by many other researchers [8,9].

Higher-bandgap a-Si:H variants would clearly be beneficial in the production of high-performance top cells, but film quality should also be considered concurrently. Fig. 3(b) shows the Si–H_2 bonding ratio of a-Si:H as a function of the H_2 dilution ratio. The Si–H_2 bonding ratio was determined using Fourier transform infrared (FT-IR) spectroscopy on glass substrates. This ratio is defined as $I_{2100}/(I_{2000}+I_{2100})$, taking into account the FT-IR peak approximately 2000–2100 cm^{-1}, which denotes the Si–H stretching mode. It has been reported that the Si–H_2 ratio in an a-Si:H film correlates well with the quality of the film [10]. From Fig. 3(b), it is clear that the Si–H_2 bonding ratio begins to increase at a lower H_2 dilution condition than was associated with the onset of the μc-Si:H transition regime in Fig. 3(a). Analyzing the relationship between the bandgap of the a-Si:H films and the Si–H_2 bonding ratio, Fig. 3(c) suggests that there is a critical H_2 dilution ratio at which the high quality of an a-Si:H film is retained. A bandgap level near 1.74 eV is expected to exhibit both high quality and a large bandgap.

Fig. 4 presents the open-circuit voltage (V_{oc}) and short-circuit current (J_{sc}) measured in p–i–n single junction cells with various intrinsic layers, as described in the previous section. As the a-Si:H bandgap increases, V_{oc} increases by a total of 0.99 V up to a bandgap value of 1.734 eV, after which it is saturated and slightly decreases with increasing bandgap. An increased bandgap in the intrinsic layer would understandably improve the V_{oc} in an a-Si:H cell, and concurrently weaken the light absorption ability. However, in the very-high hydrogen-dilution regime, the formation of μc-Si:H causes poor film quality, as verified in Fig. 3(b) and (c). Therefore, past this critical point, the V_{oc} of an a-Si:H solar cell does not increase further and the tendency of J_{sc} to decline is abruptly intensified as the bandgap of the a-Si:H layer exceeds 1.73 eV (Fig. 4(b)). This result is also consistent with previous studies [9,11] that report a critical point after which the V_{oc} performance of a-Si:H solar cells deteriorates. In our work, we have successfully introduced a very simple and effective method to detect this transition point via FT-IR measurement.

To obtain the highest cell efficiency, the component cells of a triple-junction structure must be individually optimized. To produce an optimized top cell for adoption in a triple-junction system, an a-Si:H intrinsic layer with a bandgap of 1.734 eV, near the observed critical point, was selected. As a result, an improved top cell (V_{oc}=1.00 V, J_{sc}=15.3 mA/cm^2, and F.F.=0.73) was successfully achieved through further technical optimizations, including p/i interface control, TCO/p interface control and wide bandgap p-type a-SiC:H development.

2.3. An a-SiGe:H solar cell with a new window layer: double p-type a-SiC:H

Hydrogenated amorphous silicon–germanium (a-SiGe:H) materials have the advantage of bandgaps that can be easily adjusted by controlling the Si/Ge ratio. The bandgap of an a-SiGe alloy can be controlled continuously between 1.1 eV and 1.7 eV by changing the Ge content of the alloy. This material has therefore been widely used as a middle or bottom cell absorber layer for multi-junction thin-film solar cells due to its narrow bandgap [12,13]. In this work, the a-SiGe:H layer was applied to the light-absorbing materials of the middle cells within triple-junction solar cell structures.

As a result of its wide optical bandgap and straightforward doping properties, p-type hydrogenated amorphous silicon carbide (a-SiC:H) has been implemented as a p-doping layer as well as a window layer, which is responsible for transmitting sub-bandgap light into the light absorber layer [14]. The effective introduction of photons into the absorbing layer through the wide bandgap of p-type a-SiC:H increases the value of J_{sc}. Another effect of a wide-bandgap p-layer is the formation of an effective blocking barrier for electrons at the p/i interface [15]. However, this blocking barrier results in the deterioration of the fill factor (F.F.) of the solar cell due to hindered hole-carrier flows at the p/i interface [16]. It is clear that the wider bandgap of a p-type a-SiC:H has the potential to lead to a higher V_{oc}; however, the wider bandgap doping layer also gives rise to the higher blocking barrier at the p/i interface and a lower conductivity, resulting in F.F. deterioration. Therefore, the optical bandgap of a p-type a-SiC:H layer for an a-SiGe:H solar cell is often limited due to the inherent trade-off between the optical properties and electrical properties.

In this work, we have introduced a double p-type a-SiC:H layer to mitigate this issue and to improve solar cell performance. The p-type a-SiC:H films were deposited via a RF-PECVD method with a gas mixture of H_2, SiH_4, CH_4, and B_2H_6 at a substrate temperature of 180 °C. The optical parameters, such as the optical bandgap and film thickness, were determined from ellipsometry measurements by Tauc–Lorentz fitting, and the dark conductivities were measured laterally on the coplanar electrodes. A combination of wide- and narrow-bandgap p-type a-SiC:H layers was adopted to

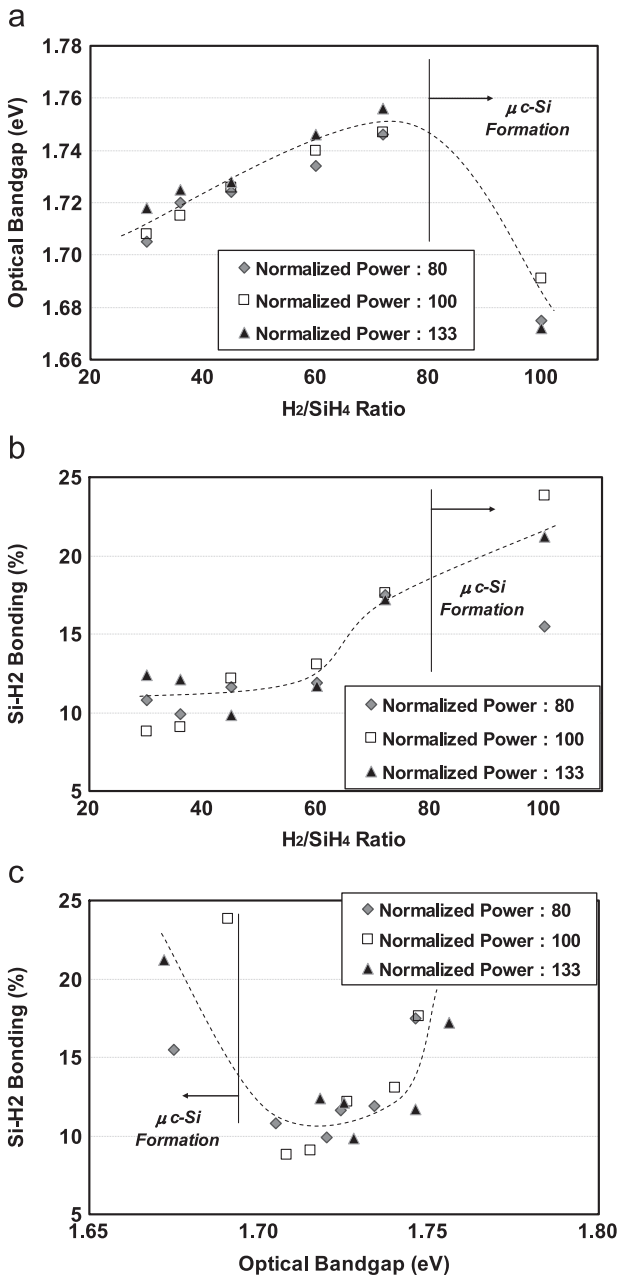

Fig. 3. Variation of (a) optical bandgap and (b) Si–H_2/(Si–H+Si–H_2) bonding ratio measured by FT-IR for intrinsic a-Si:H layers as a function of H_2/SiH_4 gas flow ratio and RF Power (Normalized) during the PECVD process. All films have the same controlled thickness of 100 nm. (c) Indicates the relationship between the optical bandgap and the Si–H_2 bonding ratio for the intrinsic a-Si:H layers.

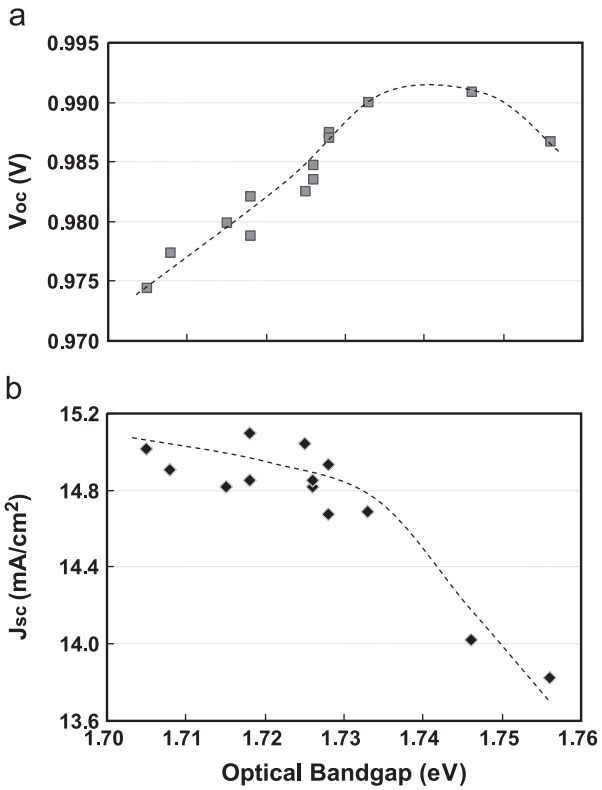

Fig. 4. Open-circuit voltage (V_{oc}) and short-circuit current (J_{sc}) for a-Si:H single junction p–i–n solar cells, plotted as a function of the intrinsic-layer optical bandgap.

increase V_{oc} and other parameters, such as F.F. and J_{sc}, in the solar cells. We deposited a set of p-type a-SiC:H films on glass substrates and investigated their optical/electrical properties. The dark conductivities and optical bandgaps of these p–a-SiC:H films are shown in Fig. 5. The optical bandgaps of the p-type a-SiC:H films increased from 1.91 eV to 2.05 eV with increasing carbon content in the films. Investigating the p-type a-SiC:H layers labeled A, B and C when each was used as the window layer of a-SiGe:H solar cell, layer A exhibited the highest F.F. and the lowest V_{oc} among three solar cells. On the other hand, layer C exhibited exactly the opposite tendencies as A did, while layer B exhibited intermediate values for the parameters F.F. and V_{oc}. For this reason, layer B was used as the window layer for an a-SiGe:H solar cell. Its solar cell performance is shown in Table 1.

In order to integrate both the advantage of a higher V_{oc} associated with a wider bandgap and a higher F.F. associated with a narrower bandgap in the window layer, combinations of multiple layers were investigated. As shown in Table 1, we prepared four p-type doping layers with single or double p-type a-SiC:H layers, then implemented these layers on a-SiGe:H solar cells. Comparison of the A/B and B/A structures shows that a p-type a-SiC:H layer with a narrower bandgap results in an increase in F.F. only if it is situated on the p/i interface side (not on the TCO side). Comparing the B/A and C/A structures, the p-type a-SiC:H layer, which has a wider bandgap, increases the V_{oc} of the solar cell when it is situated at the TCO/p side. Fig. 6 shows a schematic band diagram of an a-SiGe:H cell with a double p-a-SiC:H layer. A p-type a-SiC:H layer with a narrow bandgap can effectively lower the band barrier at the p/i interface, which consequently leads an improvement in F.F. At the same time, a p-type a-SiC:H layer with a wide bandgap deployed on the TCO/p side can retain its high intrinsic potential, resulting in an improved V_{oc} level. Through this investigation, we have successfully verified that a hole carrier flow at the p/i interface side, not at the TCO/p side, has a decisive effect on the value of F.F. in an a-SiGe:H solar cell. This scheme has been implemented effectively in a triple-junction solar cell and contributed to its improved conversion efficiency.

2.4. A high-performance μc-Si:H bottom cell with a wide-bandgap p-type doping layer

The development of hydrogenated microcrystalline silicon (μc-Si:H) is now progressing rapidly. In 1996, Meier and colleagues reported a high conversion efficiency for an a-Si:H/μc-Si:H tandem solar cell, which they named the "micromorph" solar cell [17]. Microcrystalline silicon can exhibit excellent photovoltaic properties. Its main benefits are that it shows no or less photo-

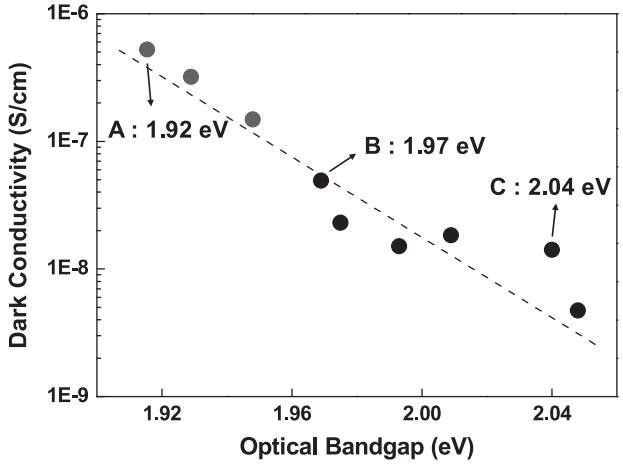

Fig. 5. Optical bandgaps and dark conductivities of various p-type a-SiC:H layers with different carbon contents. The lines are guides for the eye.

Table 1
J–V characteristics of a-SiGe:H single junction solar cells fabricated with single and double p-type a-SiC:H layers, measured under AM1.5 illumination. The 'A/B' stack denotes a double a-SiC:H layer comprised of an 'A' layer on the TCO side and a 'B' layer on the a-SiGe:H side.

p-a-SiC:H stack	Bandgap (eV)	Thickness (nm)	Eff. (%)	V_{oc} (V)	J_{sc} (mA/cm^2)	F.F.
B	1.97	12	10.85	0.740	22.87	0.641
A/B	1.91/1.97	4/8	10.77	0.743	22.76	0.637
B/A	1.97/1.91	4/8	10.99	0.736	22.83	0.654
C/A	2.04/1.91	4/8	11.18	0.746	22.88	0.655

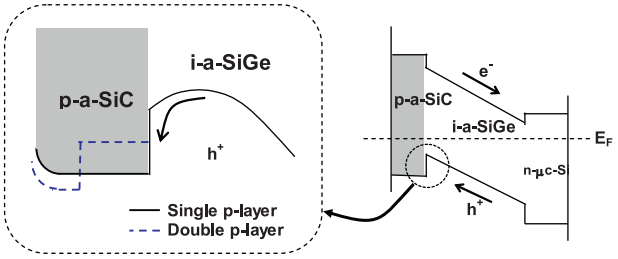

Fig. 6. Schematic band diagram of an a-SiGe:H cell with single and double p-type a-SiC:H layers. The double p-type a-SiC:H layer can lower the energy barrier between the p-type a-SiC:H and the intrinsic a-SiGe:H layers..

degradation and that it presents a higher J_{sc}. However, μc-Si:H solar cells do present a drawback in their lowered V_{oc} values, limiting the efficiency of the cells. The value of V_{oc} is sensitive to the p-type doping layer [18,19], and the requirements for this window layer are p-type silicon-based thin-films with a wide bandgap and a high conductivity. Hydrogenated microcrystalline silicon carbide (μc-SiC:H) and microcrystalline silicon oxide (μc-SiO:H) films are well known as wide-bandgap and high-conductivity materials [20–22]. Previous research has reported that the microcrystalline alloys show potential as wide-bandgap materials to improve V_{oc} [20–22].

We fabricated the μc-Si:H solar cell on the texture-etched ZnO:Al substrates (see Section 2.1). The thickness of cells was maintained at 1.6 μm, and cells were prepared in the p–i–n configuration by plasma-enhanced chemical vapor deposition (PECVD). The details of the PECVD deposition are similar to those reported previously [23,24]. To compare effectively the optical properties of various microcrystalline-based thin-films, the optical bandgap of E_{03} (the energy level at which the absorption coefficient reaches a

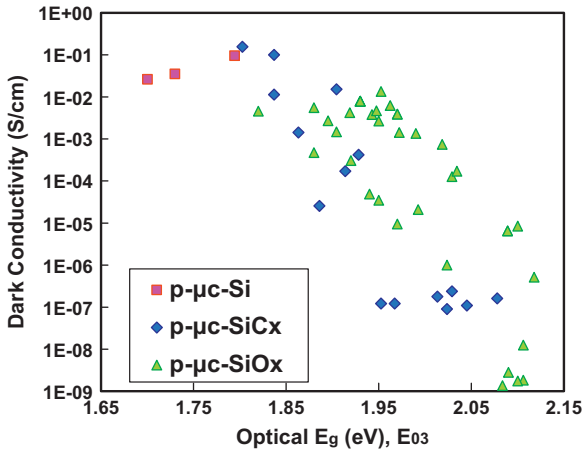

Fig. 7. Optical bandgaps (E_{03}) and dark conductivities for various p-type microcrystalline silicon alloys including μc-Si:H, μc-SiC$_x$:H, and μc-SiO$_x$:H. The p-type μc-SiO$_x$:H film has a wider, more beneficial optical bandgap than the conventional p-type μc-Si:H or μc-SiC$_x$:H films.

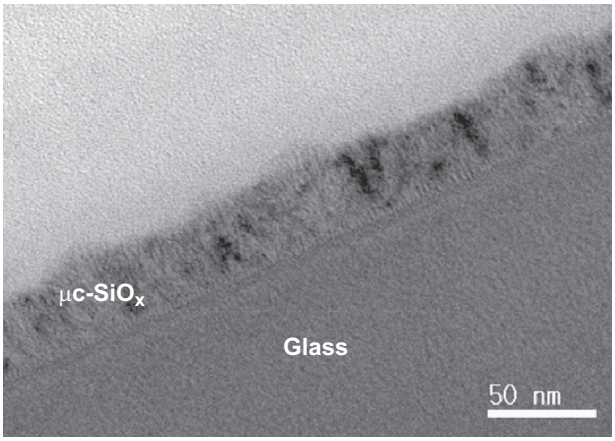

Fig. 8. A bright-field TEM cross-sectional image of a p-type μc-SiO$_x$:H film grown on a glass substrate. The p-type μc-SiO$_x$:H film appears as a two-phase mixture composed of black precipitates along the growth direction and a gray matrix material.

value of 10^3 cm^{-1}) was selected to minimize a measurement error. Fig. 7 shows the optical and electrical properties of the p-type doping layers using μc-Si:H, μc-SiC$_x$:H, and μc-SiO$_x$:H. Various p-type μc-Si(C,O)$_x$ layers were prepared by using gaseous mixtures of H_2, CO_2, CH_4, SiH_4, and B_2H_6 and by varying of PECVD parameters to investigate the layer properties. With increasing carbon or oxygen content, the optical bandgap tends to increase and the dark conductivity tends to decrease. The optical bandgap of the μc-SiO$_x$:H layer reaches a value of nearly 2.12 eV. In contrast, the p-type μc-Si:H and μc-SiC$_x$:H layers reach values of 1.8 eV and 2.08 eV, respectively. It is therefore apparent that the p-type μc-SiO$_x$:H layers exhibit wider optical bandgaps, which is an advantage over the p-type μc-Si:H and μc-SiC$_x$:H layers.

To confirm the characteristics of the p-type μc-SiO$_x$:H layers, AES (Auger electron spectroscopy) and TEM (Transmission electron microscopy) analyses were performed. A TEM cross-sectional image of a p-type μc-SiO$_x$:H layer is presented in Fig. 8. A two-phase mixture comprised of black precipitates (μc-Si:H) and a gray matrix (a-SiO$_x$:H) can be observed clearly. This identification of a two-phase mixture is identical to our previous analysis by Raman spectroscopy [24]. The composition of this layer was analyzed by AES. The oxygen was effectively incorporated with silicon, and the atomic ratio of oxygen varied from 3% to 11% along with various PECVD deposition conditions in our experiments.

Table 2
Cell parameters achieved for single-junction μc-Si:H solar cells with a conventional μc-Si:H p-doping layer and the new μc-SiC_x:H/μc-SiO_x:H p-doping layer.

p-doping layer (E_{03}, dark σ)	μc-Si:H (1.79 eV, 9.5E−2 S/cm)	μc-SiC_x:H (1.93 eV, 4.2E−4 S/cm)	μc-SiO_x:H (2.10 eV, 8.4E−6 S/cm)
Eff. (%)	8.9	9.8	10.4
J_{sc} (mA/cm^2)	25.3	25.8	26.1
V_{oc} (V)	0.51	0.52	0.54
F.F. (%)	0.69	0.72	0.73

To investigate the effects of p-type μc-$Si(C,O)_x$ layers on single-junction μc-Si:H solar cells, various p-type μc-$Si(C,O)_x$ layers in Fig. 7 were adopted as window layers. As shown in Table 2, a p-type μc-SiO_x:H window layer with a moderate conductivity and a wide optical bandgap showed the highest conversion efficiency. The adoption of this wide bandgap p-doping layer could lead to higher values of V_{oc} for μc-Si:H thin-film solar cells, as well as higher J_{sc} values resulting from the reduced absorption loss in the short-wavelength region. Recently, Biron et al. [25] has reported two scenarios explaining the V_{oc} enhancement brought by the μc-SiO_x:H window layers in a-Si:H n–i–p solar cells. Unfortunately, in case of our μc-Si:H p–i–n solar cells, the origin for the enhanced V_{oc} in the μc-SiO_x:H window layer has not been distinguished exactly between the increased built-in voltage (V_{bi}) and the reduced recombination at p/i interface. Further investigation should be performed for the clear understanding about the origin of V_{oc} improvement in this study.

Consequently, we obtained an optimal p-type window layer with improved properties, including a widened optical bandgap and a reduced optical loss. These results indicate that a p-type μc-SiO_x:H layer with a wide bandgap is suitable for application as the window layer of the bottom cell in a triple-junction solar cell as well as in a single-junction μc-Si:H thin-film solar cell.

2.5. The application of n-type microcrystalline silicon oxide (μc-SiO_x:H) in a high-performance back reflector

For high-efficiency triple-junction solar cells, light trapping is necessary to obtain a high current density, as the absorption coefficient of μc-Si:H is not sufficient in the long-wavelength near-infrared region. To achieve more efficient light trapping and higher current density in μc-Si:H, the parasitic absorption losses occurring at the back and front electrodes should be minimized by optimizing the back reflector configuration and/or the front electrode TCO material [26,27].

Among the various constituent elements necessary for efficient light trapping, the choice of material for a back reflector plays an important role in improving the light utilization efficiency. Thus far, the application of Al-doped zinc oxide (ZnO:Al) films to the back reflectors of thin-film Si solar cells to increase the reflection of light from the back contact has received significant attention [26–29]. The ZnO:Al layer has a refractive index of approximately 2.0, which is low compared to the refractive index of μc-Si:H ($n=3.8$), allowing efficient total reflection at the interface between μc-Si:H and the ZnO:Al back reflector. Typically, a ZnO:Al and silver double layer is used as the back reflector, providing a textured rough surface and thereby increasing the light path inside a μc-Si:H solar cell and reducing plasmon absorption at the interface of a silicon/metal [30]. To improve the reflective performance of the back reflector further, the refractive index of the back reflector material should be minimized as much as possible to provide strong total reflection [35].

To apply a low-refractive-index material, we investigated the possibility of using an n-type microcrystalline silicon oxide (μc-SiO_x:H) back reflector instead of an ZnO:Al reflector. A number of studies regarding the n-type μc-SiO_x:H layer and its application in thin-film Si solar cells have been reported [3,31–37]. The n-type μc-SiO_x:H was successfully applied to an intermediate reflector layer in double- or triple-junction solar cells [31–33], and was also proposed as novel designs of back reflector [36,37]. In this study, we investigated the electrical and optical properties of n-type μc-SiO_x:H films and attempted to verify the advantages of using a μc-SiO_x:H layer as a new back reflector material in thin-film Si solar cells.

The n-type μc-SiO_x:H layers were deposited by RF-PECVD from a gas mixture of SiH_4, H_2, diluted PH_3, and CO_2. Through Raman spectroscopy analysis, it was determined that the n-type μc-SiO_x:H layer consisted of a phase mixture of μc-Si:H with amorphous silicon oxide (a-SiO_x:H). This result is consistent with previous studies [31–33] and our TEM result for p-type μc-SiO_x:H (see Fig. 8).

Fig. 9 shows the variation of the refractive index measured at a wavelength of 850 nm and the lateral electrical resistivity for both a ZnO:Al layer deposited by an RF sputtering process and an n-type μc-SiO_x:H layer deposited by the PECVD process. Most of the n-type μc-SiO_x:H samples analyzed in this work exhibited lower refractive indices than did conventional ZnO:Al films. The electrical resistivities of these films were considerably higher than the value of $9.5\times10^{-4}\,\Omega$ cm reported for ZnO:Al, but it should be noted that the conductivities were measured laterally on the coplanar electrodes and that the n-type μc-SiO_x:H films showed anisotropic conductivities between the vertical and lateral directions [32,33]. Three different n-type μc-SiO_x:H layers were

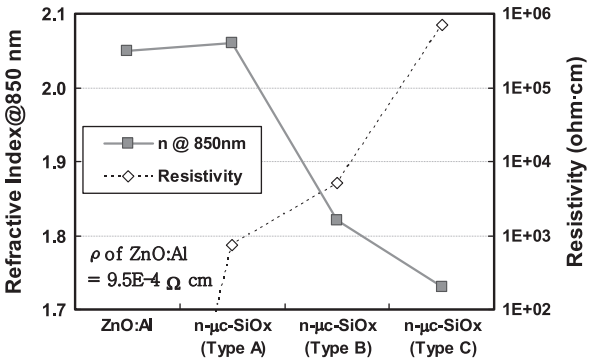

Fig. 9. Variation of refractive index measured at a wavelength of 850 nm, as well as lateral electrical resistivity, for 100-nm thick ZnO:Al and n-doped microcrystalline silicon oxide layers.

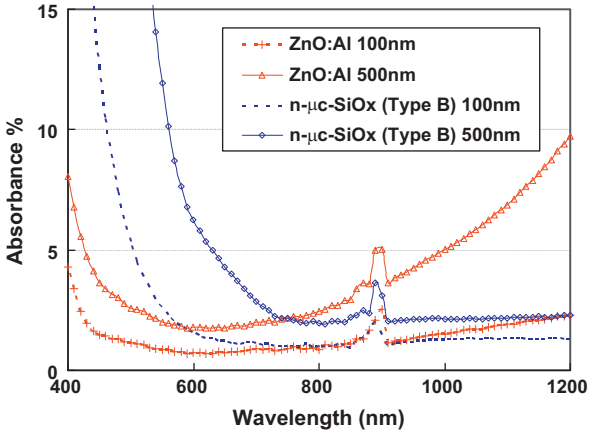

Fig. 10. Absorbance spectra for ZnO:Al and n-type μc-SiO_x:H films, each at two thicknesses (100 and 500 nm), evaluated as (1-T–R) from a spectrophotometer with an integrating sphere (T=Transmittance and R=Reflectance). The data include the absorption portion of 0.7-mm thick C1737 Corning glass substrates.

produced by controlling gas flux ratios between SiH_4, CO_2 and H_2 during PECVD deposition. These ratios control the consequent phase fraction of silicon complexes within a-SiO_x:H matrix, thereby determining the opto-electrical properties of the three μc-SiO_x:H layers. Of these μc-SiO_x:H layers, type B was selected as the optimal condition for the back reflector of a μc-Si:H single-junction cell and/or triple-junction structure, due to its low refractive index (less than 1.85). Type C layers exhibited a refractive index below 1.75, which is too low for application as a thick back reflector with a thickness over 300 nm, and also resulted in degraded solar cell performance due to the increased series resistance caused by the high electrical resistivity of these layers.

Fig. 10 presents absorption spectra of selected n-type μc-SiO_x:H (Type B) and ZnO:Al films with thicknesses of 100 nm and 500 nm.

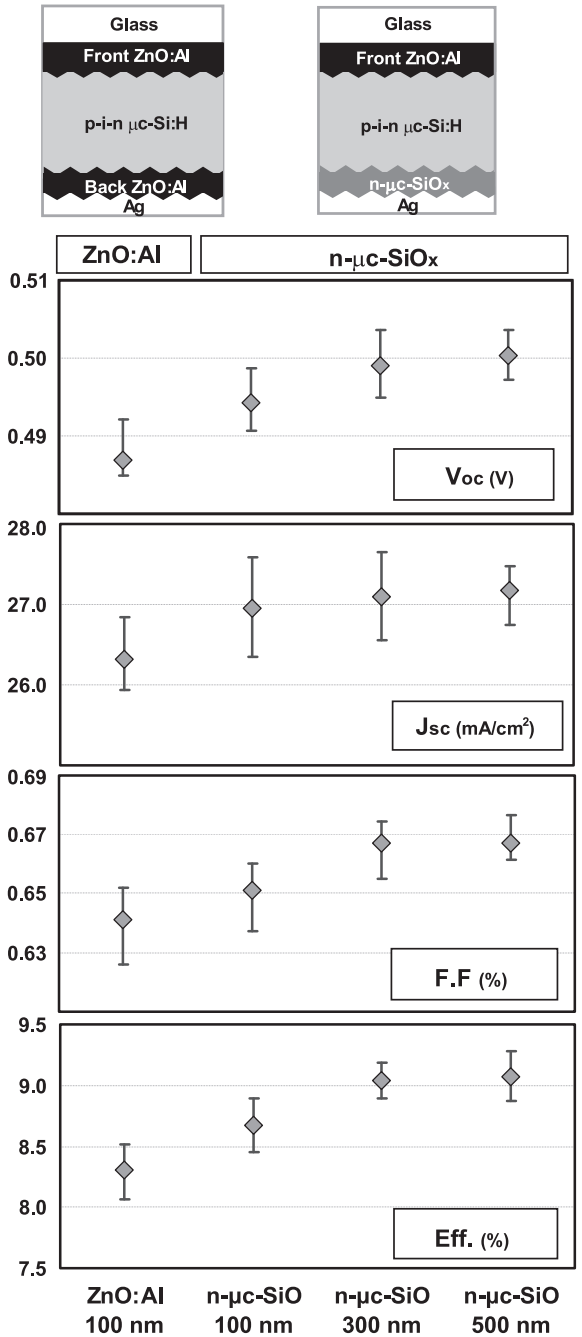

Fig. 11. Photo *J–V* characteristics of the best microcrystalline silicon p–i–n solar cells prepared with the conventional ZnO:Al layer and the new, thick n-type μc-SiO_x:H back reflector electrodes.

The selected μc-SiO_x:H film has a refractive index of 1.82. For an identical film thickness, the n-type μc-SiO_x:H layer exhibits an absorption edge that is shifted toward longer wavelengths in the range of 500–600 nm. However, it is expected that this edge shift should not affect the J_{sc} performance of μc-Si:H solar cells because the incident light in the blue region is entirely absorbed within the intrinsic μc-Si:H layer before reaching the μc-SiO_x:H back reflector. Additionally, the lower absorption of n-type μc-SiO_x:H in the near-IR region compared with that of ZnO:Al could reduce the parasitic absorption loss at the back reflector.

Fig. 11 shows the performance of the fabricated μc-Si:H solar cells using an n-type μc-SiO_x:H layer as a back reflector, for several reflector thicknesses. It is apparent from the graph that all of the cell parameters increased drastically for the sample utilizing the μc-SiO_x:H reflector. As mentioned in the previous sections, the n-type μc-SiO_x:H back reflector has a lower refractive index and lower absorbance in the near-IR region than does the ZnO:Al reflector. Therefore, its superior optical properties could improve the utilization of long-wavelength light within a thin-film solar cell. More importantly, as shown in Fig. 11, μc-Si:H cells with back reflectors thicker than 100 nm did not show any degraded J_{sc} performance. The current density was even slightly increased, resulting from the strong reflectivity and low absorbance of μc-SiO_x:H. It is remarkable that both the V_{oc} and F.F. of samples using n-type μc-SiO_x:H back reflectors are superior to those using ZnO:Al. Furthermore, the performance gains in both V_{oc} and F.F. were more obvious when thicker back reflectors were used. These interesting performance gains might be related to the anisotropic electrical characteristics of μc-SiO_x:H that have been reported in other works [32,33]. We expect that the higher electrical resistivity of this material in the planar direction as compared to the film growth direction could reduce the shunt current at the back contacts of the μc-Si:H cells. These effects are magnified as the thickness of the n-type μc-SiO_x:H layer increases.

3. Triple-junction integration technologies

3.1. Enhanced current matching using a high-performance intermediate reflector layer

A triple-junction thin-film solar cell consisting of a top cell (a-Si:H), a middle cell (a-SiGe:H or μc-Si:H) and a bottom cell (μc-Si:H) is a promising candidate for a high-efficiency solar cell. To achieve this high efficiency, current matching between each subcell is required because the short-circuit current (J_{sc}) in multi-junction solar cells is limited by the lowest J_{sc} of the subcells. One widely used solution for enhanced current matching is the introduction of an intermediate reflector layer that enhances the J_{sc} of the top and/or middle cells by reflecting non-absorbed photons into one or both of them. The intermediate reflector is usually made of a material with a lower refractive index than silicon to create an index contrast that increases the reflection of light at the Si/intermediate-reflector interface. Recently, n-type μc-SiO_x:H has been adopted as a material for the intermediate reflector layer because of its low refractive index, its low absorbance in the long-wavelength region, and the fact that no additional laser scribe is needed for a monolithic interconnection when fabricating modules with this material [31,32].

In this study, n-type μc-SiO_x:H intermediate reflector layers with various refractive indices were applied in the design of a triple-junction (a-Si:H/a-SiGe:H/μc-Si:H) thin-film Si solar cell. These intermediate reflector layers were introduced between the middle (a-SiGe:H) and bottom (μc-Si:H) cells to compensate for the middle cell current.

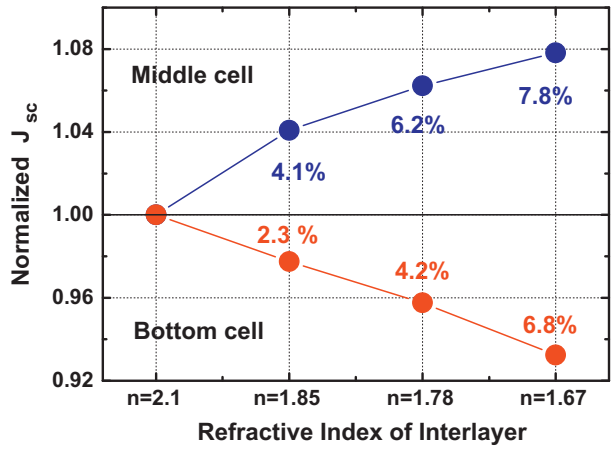

Fig. 12. Normalized J_{sc} of middle and bottom cells for intermediate reflector layers of various refractive indices.

The effect of current matching between the middle and bottom cells was investigated, and Fig. 12 shows the relationship between the J_{sc} of the middle and bottom cells and refractive index of an intermediate reflector layer of fixed thickness for each subcell. We controlled the refractive index of the intermediate reflector layer in the range of 1.67–2.1 by adjusting the PECVD deposition conditions, such as the SiH_4/CO_2, SiH_4/H_2, SiH_4/PH_3 gas ratios, the plasma power and the working pressure.

As the refractive index of intermediate reflector layer decreased from 2.1 to 1.67, the gain of the middle cell current density increased up to a value of 7.8%. On the other hands, the loss of the bottom cell current density is 6.8% for a reflector-layer refractive index of 1.67. The figure of merit, the J_{sc} gain in the triple-junction, is maximized (+2%) at $n=1.78$, and decreases to +1% at $n=1.67$. To maximize the total current in the triple-junction system, a refractive index of 1.78 might be selected as an optimal condition. However, it should be noted that the intermediate reflector layer with the lowest refractive index, $n=1.67$, can reduce the thickness of the middle absorption layer (a-SiGe:H) due to its strong reflection effect. We found that the open-circuit voltage (V_{oc}) and fill factor (F.F.) of the triple-junction cell improved remarkably as the thickness of the a-SiGe:H absorbing layer decreased. We have therefore optimized the triple-junction cells under the condition of $n=1.67$. As already mentioned in Section 2.5, the low conductivity ($< 5\times10^{-6}$ S/cm) of n-type μc-SiO_x:H layer often led to the degradation of F.F. in the solar cells when its thickness exceeded 300 nm or more. But if the thickness of n-type μc-SiO_x:H layer was not so thick (below 100 nm in our case), it was confirmed that even if the conductivity reached 5×10^{-7} S/cm, the layer could be applied without the degradation of F.F. in the solar cells.

Fig. 13 shows the (a) photo *J–V* characteristics and (b) External quantum efficiency (EQE) of the best a-Si:H/a-SiGe:H/μc-Si:H triple-junction thin-film Si solar cell prepared with a low-refractive-index intermediate reflector ($n=1.67$). The initial efficiency of 16.1% ($V_{oc}=2.20$ V, $J_{sc}=9.98$ mA/cm^2, and F.F.$=0.732$) was successfully achieved in a 1 cm^2 triple-junction solar cell fabricated with the high-performance TCO and optimized component layers, including new wide-bandgap doping layers and highly reflective back/intermediate reflector layers.

3.2. *Superior stabilized performance using a modified triple-junction structure*

It is well-known that the electrical properties of Si:H-based materials suffer deterioration under light exposure. This light-induced degradation behavior is known as the Staebler–Wronski effect [38]. The light-induced degradation of a-Si:H-based solar cells depends strongly on the thickness of the light absorber layers. On the other hand, either no or less light-induced degradation was observed in the electrical properties of μc-Si:H depending on the deposition conditions [39–41]. It was therefore highly advantageous to use a μc-Si:H bottom cell in multi-junction solar cells in order to improve the efficiency further and minimize the light-induced degradation.

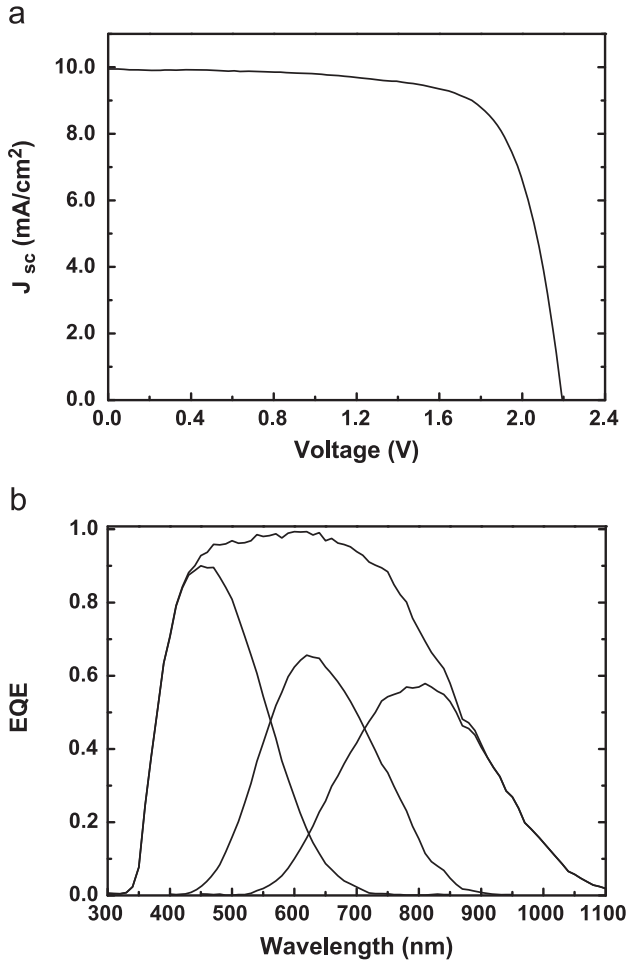

Fig. 13. (a) Photo *J–V* characteristics (initial property) and (b) External quantum efficiency (EQE) of the best a-Si:H/a-SiGe:H/μc-Si:H triple-junction p–i–n solar cell prepared with a low-refractive-index intermediate reflector layer.

We here present two types of triple-junction solar cells to compare their stabilized performances. One type is a triple-junction solar cell with an amorphous middle cell, a-Si:H/a-SiGe:H/μc-Si:H, and the other is a triple-junction solar cell with microcrystalline middle cell, a-Si:H/μc-Si:H/μc-Si:H. The μc-Si:H used in the middle cell has just the same p–i–n structure with the μc-Si:H in the bottom cell except the thickness of intrinsic layer. Table 3 shows the results of light-induced degradation for the various triple-junction structures. When a-SiGe:H is used in the middle cell, the efficiency degradation ratio after 1000 h light soaking was approximately 18% in the case of an a-SiGe:H layer with 220 nm thickness, and 15% in the case of a layer with 180 nm thickness. As mentioned above, the solar cell performance deteriorated further as the thickness of the a-Si:H based layer increased. This deterioration was mainly caused by the deterioration of the F.F. in the cells. However, in the cases for which μc-Si:H was used as a middle cell, the degradation ratio was only approximately 4%, even after 1000 h light soaking. Although the

Table 3
Light-induced degradation of triple-junction silicon thin-film solar cells with different cell structures and middle cell thicknesses. The light-soaking test was performed under the standard condition of 100 mW/cm^2 white light at 50 °C for 1000 h.

Sample no.	Middle cell (intrinsic)	Thickness (intrinsic)	LID ratio of F. F. (%)	LID ratio of efficiency (%)
TA	a-SiGe:H	220 nm	13	18
TB	a-SiGe:H	180 nm	10	15
TC	μc-Si:H	1.2 μm	3	4
TD	μc-Si:H	0.9 μm	3	4

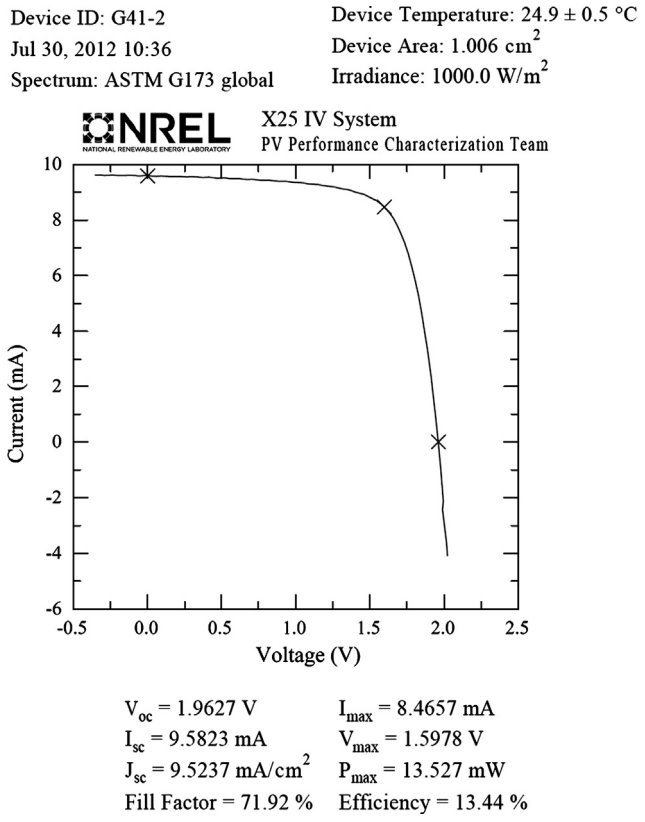

Fig. 14. The established performance of the a-Si:H/μc-Si:H/μc-Si:H triple-junction solar cell after 1000 h light soaking. This new record was confirmed by NREL.

initial efficiencies of the triple-junction solar cells with μc-Si:H middle cells were somewhat lower than those triple-junction cells with a-SiGe:H middle cells, the stabilized efficiencies were significantly improved by using as a middle cell material μc-Si:H, which has superior stability under light soaking. Finally, as shown in Fig. 14, a maximum stabilized efficiency of 13.44% was achieved and confirmed by NREL for a triple-junction a-Si:H/μc-Si:H/μc-Si:H thin-film solar cell that was 1 cm^2 in size. Light soaking was performed under the standard condition of 100 mW/cm^2 white light at 50 °C for 1000 h.

4. Conclusions

To produce high-efficiency thin-film Si solar cells, we developed triple-junction solar cell structures with enhanced solar spectrum utilization. As a result, an initial efficiency of 16.1% (a-Si:H/a-SiGe:H/μc-Si:H, in-house measurement) and a stabilized efficiency of 13.4% (a-Si:H/μc-Si:H/μc-Si:H, confirmed by NREL) were successfully achieved for a small-area triple-junction solar cell with dimensions of 1 cm × 1 cm. We believe that our new world record for a p–i–n stacked thin-film Si solar cell can be improved by further developments in novel light trapping technology and high-quality wide-bandgap materials. Additionally, a high-power module that is 1.1 m × 1.3 m in size is under development using the high-efficiency triple-junction cell technologies described in this article.

References

[1] J. Bailat, L. Fesquet, J.-B. Orhan, Y. Djeridane, B. Wolf, P. Madliger et al.,, Recent Developments of high-efficiency micromorph tandem solar cells in KAI-M PECVD reactors, in: Proceeding of the 25th European Photovoltaic Solar Energy Conference, Valencia, Spain, 2010, pp.2720–2723.
[2] M. Konagai, Present status and future prospects of silicon thin-film solar cells, Japanese Journal of Applied Physics 50 (2011) 030001-1–030001-12.
[3] B. Yan, G. Yue, L. Sivec, J. Yang, S. Guha, C.-S. Jiang, Innovative dual function nc-SiO_x:H layer leading to a > 16% efficient multi-junction thin-film silicon solar cell, Applied Physics Letters 99 (2011) 113512-1–113512-3.
[4] C. Agashe, O. Kluth, J. Hüpkes, U. Zastrow, B. Rech, M. Wuttig, Efforts to improve carrier mobility in radio frequency sputtered aluminum doped zinc oxide films, Journal of Applied Physics 95 (2004) 1911–1917.
[5] O. Kluth, G. Schöpe, J. Hüpkes, C. Agache, J. Müller, B. Rech, Modified Thornton model for magnetron sputtered zinc oxide: film structure and etching behavior, Thin Sold Films 442 (2003) 80–85.
[6] Y. Nasuno, M. Kondo, A. Matsuda, Effect of substrate surface morphology on microcrystalline silicon solar cells, Japanese Journal of Applied Physics 40 (2001) L303–L305.
[7] M. Python, E.V. Sauvain, J. Bailat, D. Dominé, L. Fesquet, A. Shah, C. Ballif, Relation between substrate surface morphology and microcrystalline silicon solar cell performance, Journal of Non-Crystalline Solids 354 (2008) 2258–2262.
[8] C.R. Wronski, B. Von Roedern, A. Kolodziej, Thin-film Si:H-based solar cells, Vacuum 82 (2008) 1145–1150.
[9] J. Koh, Y. Lee, H. Fujiwara, C.R. Wronski, R.W. Collins, Optimization of hydrogenated amorphous silicon p–i–n solar cells with two-step i layers guided by real-time spectroscopic ellipsometry, Applied Physics Letters 73 (1998) 1526–1528.
[10] M. Kondo, T. Matsui, Y. Nasuno, H. Sonobe, S. Shimizu, Key issues for fabrication of high quality amorphous and microcrystalline silicon solar cells, Thin Solid Films 501 (2006) 243–246.
[11] S. Guha, Thin film silicon solar cells grown near the edge of amorphous to microcrystalline transition, Solar Energy 77 (2004) 887–892.
[12] S. Guha, J. Yang, A. Banerjee, Amorphous silicon alloy photovoltaic research—present and future, Progress in Photovoltaics: Research and Applications 8 (2000) 141–150.
[13] Y. Ichikawa, T. Yoshida, T. Hama, H. Sakai, K. Harashima, Production technology for amorphous silicon-based flexible solar cells, Solar Energy Materials and Solar Cells 66 (2001) 107–115.
[14] Y. Tawada, H. Okamoto, Y. Hamakawa, a-SiC/a-Si:H Heterojunction solar cell having more than 7.1% conversion efficiency, Applied Physics Letters 39 (1981) 237–239.
[15] Y. Tawada, K. Tsuge, M. Kondo, H. Okamoto, Y. Hamakawa, Properties and structure of a-SiC:H for high-efficiency a-Si solar cell, Journal of Applied Physics 53 (1982) 5273–5281.
[16] S.Y. Myong, S.S. Kim, K.S. Lim, Improvement of pin-type amorphous silicon solar cell performance by employing double silicon-carbide p-layer structure, Journal of Applied Physics 95 (2004) 1525–1530.
[17] D. Fischer, S. Dubail, J.A.A. Selvan, N.P. Vaucher, R. Platz, C. Hof, U. Kroll, J. Meier, P. Torres, H. Keppner, N. Wyrsch, M. Goetz, A. Shah, K.-D. Ufert, The "micromorph" solar cell: extending a-Si:H technology towards thin film crystalline silicon, in: Proceedings of 25th IEEE Photovoltaic Specialists Conference, 1996, pp.1053–1056.
[18] J. Meier, S. Dubail, J. Cuperus, U. Kroll, R. Platz, P. Torres, J.A.A. Selvan, P. Pernet, N. Beck, N.P. Vaucher, Ch. Hof, D. Fischer, H. Keppner, A. Shah, Recent progress in micromorph solar cells, Journal of Non-Crystalline Solids 227–230 (1998) 1250–1256.
[19] Y. Nasuno, M. Kondo, A. Matsuda, Formation of interface defects by enhanced impurity diffusion in microcrystalline silicon solar cells, Applied Physics Letters 81 (2002) 3155–3157.
[20] T. Wada, M. Kondo, A. Matsuda, Improvement of V_{oc} using carbon added microcrystalline Si p-layer in microcrystalline Si solar cells, Solar Energy Materials and Solar Cells 74 (2002) 533–538.
[21] P. Sichanugrist, T. Sasaki, A. Asano, Y. Ichikawa, H. Sakai, Amorphous silicon oxide and its application to metal/n–i–p/ITO type a-Si solar cells, Solar Energy Materials and Solar Cells 34 (1994) 415–422.
[22] K. Sriprapha, N. Sitthiphol, P. Sangkhawong, V. Sangsuwan, A. Limmanee, J. Sritharathikhun, p-Type hydrogenated silicon oxide thin film deposited near amorphous to microcrystalline phase transition and its application to solar cells, Current Applied Physics 11 (2011) S47–S49.
[23] S. Kim, J. Park, H. Lee, H. Lee, S.-W. Ahn, H.-M. Lee, Microcrystalline silicon carbide p-layer with wide-bandgap and its application to single- and triple-junction silicon thin-film solar cells, Japanese Journal of Applied Physics 51 (2012) 10NB11-1–10NB11-4.

[24] S. Kim, H. Lee, J.-W. Chung, S.-W. Ahn, H.-M. Lee, n-Type microcrystalline silicon oxide layer and its application to high-performance back reflectors in thin-film silicon solar cells, Current Applied Physics 13 (2013) 743–747.
[25] R. Biron, C. Pahud, F.-J. Haug, C. Ballif, Origin of the V_{oc} enhancement with a p-doped nc-SiO_x:H window layer in n–i–p solar cells, Journal of Non-Crystalline Solids 358 (2012) 1958–1961.
[26] M. Berginski, J. Hüpkes, A. Gordijn, W. Reetz, T. Wätjen, B. Rech, M. Wuttig, Experimental studies and limitations of the light trapping and optical losses in microcrystalline silicon solar cells, Solar Energy Materials and Solar Cells 92 (2008) 1037–1042.
[27] X.D. Zhang, Y. Zhao, Y.T. Gao, F. Zhu, C.C. Wei, X.L. Chen, J. Sun, G.F. Hou, X. H. Geng, S.Z. Xiong, Influence of front electrode and back reflector electrode on the performances of microcrystalline silicon solar cells, Journal of Non-Crystalline Solids 352 (2006) 1863–1867.
[28] A.M.K. Dagamseh, B. Vet, F.D. Tichelaar, P. Sutta, M. Zeman, ZnO:Al films prepared by rf magnetron sputtering applied as back reflectors in thin-film silicon solar cells, Thin Solid Films 516 (2008) 7844–7850.
[29] G. Yue, L. Sivec, J.M. Owens, B. Yan, J. Yang, S. Guha, Optimization of back reflector for high efficiency hydrogenated nanocrystalline silicon solar cells, Applied Physics Letters 95 (2009) 263501-1–263501-3.
[30] F.-J. Haug, T. Söderström, O. Cubero, V. Terrazzoni-Daudrix, C. Ballif, Plasmonic absorption in textured silver back reflectors of thin film solar cells, Journal of Applied Physics 104 (2008) 064509-1–064509-7.
[31] A. Lambertz, T. Grundler, F. Finger, Hydrogenated amorphous silicon oxide containing a microcrystalline silicon phase and usage as an intermediate reflector in thin-film silicon solar cells, Journal of Applied Physics 109 (2011) 113109-1–113109-10.
[32] P. Buehlmann, J. Bailat, D. Dominé, A. Billet, F. Meillaud, A. Feltrin, C. Ballif, In situ silicon oxide based intermediate reflector for thin-film silicon micromorph solar cells, Applied Physics Letters 91 (2007) 143505-1–143505-3.
[33] C. Das, A. Lambertz, J. Huepkes, W. Reetz, F. Finger, A constructive combination of antireflection and intermediate-reflector layers for a-Si/μc-Si thin film solar cells, Applied Physics Letters 92 (2008) 053509-1–053509-3.
[34] M. Despeisse, G. Bugnon, A. Feltrin, M. Stueckelberger, P. Cuony, F. Meillaud, A. Billet, C. Ballif, Resistive interlayer for improved performance of thin film silicon solar cells on highly textured substrate, Applied Physics Letters 96 (2010) 073507-1–073507-3.
[35] E. Moulin, U.W. Paetzold, K. Bittkau, J. Owen, J. Kirchhoff, A. Bauer and R. Carius, Investigation of the impact of the rear-dielectric/silver back reflector design on the optical performance of thin-film silicon solar cells by means of detached reflectors, Progress in Photovoltaics: Research and Applications, http://dx.doi.org/10.1002/pip.2355, in press.
[36] P.D. Veneri, L.V. Mercaldo, I. Usatii, Improved micromorph solar cells by means of mixed-phase n-doped silicon oxide layers, Progress in Photovoltaics: Research and Applications 21 (2013) 148–155.
[37] L.V. Mercaldo, P.D. Veneri, I. Usatii, T. Polichetti, Broadband near-field effects for improved thin film Si solar cells on randomly textured substrates, Solar Energy Materials and Solar Cells 112 (2013) 163–167.
[38] D.L. Staebler, C.R. Wronski, Reverse conductivity changes in discharge-produced amorphous Si, Applied Physics Letters 31 (1977) 292–294.
[39] J. Meier, R. Fluckiger, H. Keppner, A. Shah, Complete microcrystalline p–i–n solar cell-crystalline or amorphous behavior, Applied Physics Letters 65 (1994) 860–862.
[40] F. Meillaud, E. Vallat-Sauvain, X. Niquille, M. Duubey, J. Bailat, A. Shah, C. Ballif, Light-induced degradation of thin film amorphous and microcrystalline silicon solar cells, in: Proceedings of the 31st IEEE, Orlando, FL, USA, 2005, pp.1412-1415.
[41] B. Yan, G. Yue, J.M. Owens, J. Yang, S. Guha, Light-induced metastability in hydrogenated nanocrystalline silicon solar cells, Applied Physics Letters 85 (2004) 1925–1927.